Hindawi Publishing Corporation
Journal of Thermodynamics
Volume 2012, Article ID 351968, 5 pages
doi:10.1155/2012/351968

*Research Article*

# Water Desorption Process in Room Temperature Ionic Liquid-$H_2O$ Mixtures: *N*, *N*-diethyl-*N*-methyl-*N*-(2-methoxyethyl) Ammonium Tetrafluoroborate

**Hiroshi Abe,[1] Tomohiro Mori,[1] Yusuke Imai,[1] and Yukihiro Yoshimura[2]**

[1] *Department of Materials Science and Engineering, National Defense Academy, Yokosuka 239-8686, Japan*
[2] *Department of Applied Chemistry, National Defense Academy, Yokosuka 239-8686, Japan*

Correspondence should be addressed to Hiroshi Abe, ab@nda.ac.jp

Received 5 July 2011; Accepted 7 September 2011

Academic Editor: Ramesh Gardas



A water desorption process of a mixture of room temperature ionic liquid (*N*, *N*-diethyl-*N*-methyl-*N*-(2-methoxyethyl) ammonium tetrafluoroborate) and water was investigated via simultaneous X-ray diffraction and differential scanning calorimetry (DSC) measurements, in which relative humidity was controlled by a water vapor generator. In these measurements, $H_2O$ concentration was estimated by the peak position of the *principal* peak in X-ray diffraction patterns, and the thermal property associated with a mixing state was detected by a DSC thermograph. In addition, the density of the mixture was measured as a macroscopic property. *In situ* observations revealed that the thermally unstable mixing state in the water-rich region has an important correlation with density and thermal and structural properties.

## 1. Introduction

Numerous investigations of room temperature ionic liquids (RTILs) have been performed to produce green solvents [1]. These RTILs are organic salts, which consist only of a cation and an anion. Nonmeasurable vapor pressure is considered as an outstanding feature of RTILs.

To study physicochemical properties, chemical potential and enthalpy are investigated using RTILs and water mixtures [2]. RTILs include 1-butyl-3-methylimidazolium tetrafluoroborate, $[C_4mim][BF_4]$ and 1-butyl-3-methylimidazolium iodide, $[C_4mim]I$. Here a series of cations such as 1-alkyl-3-methyl-imidazolium is expressed as $[C_nmim]$ using the alkyl chain length, *n*. Anomalies in the water-rich region were observed in excess partial molar enthalpies. Moreover, the excess molar enthalpy was examined systematically in various aqueous solutions [3]. For example, in $[C_4mim][BF_4]$, the maximum value of the excess isobaric molar heat capacity appeared at around 80 mol% $H_2O$. Considering hydrophilicity and hydrophobicity, which are determined by the chemical structure of the anion, the hydrogen bonding of water was discussed. Solubilities of various types of RTILs and additives have been recently summarized [4]. The liquid-liquid equilibrium (LLE) and the solid-liquid equilibrium (SLE) in a binary liquid system revealed the mixing states as a result of molecular interactions including a hydrogen-bond donor and acceptor. From the perspective thermodynamics, activity and enthalpy were estimated by solute heat capacity and melting temperature. Moreover, thermomorphic phase separation in RTIL-organic liquid systems was investigated by electrical conductivity, FT-Raman, and NMR measurements [5], and the LLE relative to the phase separation in binary liquids was determined. Proton dynamics in the vicinity of the phase separation were clearly distinguished in NMR spectra. Macroscopic solubilities and conductivity were correlated with molecular interactions described by FT-Raman and NMR spectroscopy. Moreover, LLE and SLE in quaternary phosphonium RTIL-based mixtures were determined [6]. RTIL was regarded as

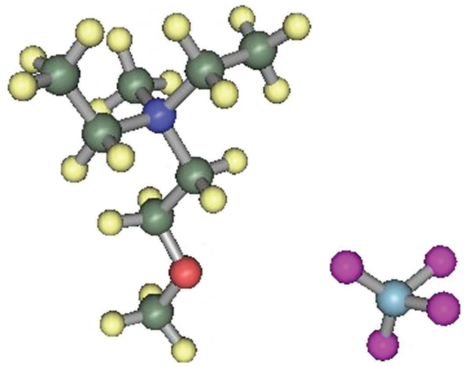

Figure 1: A [DEME] cation and a [$BF_4$] anion.

a nonimidazolium system, and the solubility was interpreted by the polar anion-solvent interaction.

Recently, a different type of RTIL *N*, *N*-diethyl-*N*-methyl-*N*-(2-methoxyethyl) ammonium tetrafluoroborate, [DEME][$BF_4$], was synthesized having a high potential for electrochemical capacitor applications [7]. The complicated SLE in the [DEME][$BF_4$]-$H_2O$ mixture, caused by various types of hydrogen bonding, was determined by simultaneous X-ray diffraction and differential scanning calorimetry (DSC) measurements [8, 9]. The bonding nature strongly depends on the local environment, that is, coordination number, molecular orientational order, and molecular packing efficiency. We recently determined that an outstanding hierarchy structure of [DEME][$BF_4$]-$H_2O$ mixtures is formed even in the liquid state [10]. On each scale, various types of anomalies appeared at respective water concentrations that included anomalous optical absorption in the UV-vis region, density fluctuation by small angle X-ray scattering, a network-forming property by the *prepeak* in the X-ray diffraction patterns, and the liquid structure by X-ray diffraction. We recently summarized a series of our researches on [DEME][$BF_4$]-$H_2O$ mixtures from the perspective of hydrogen bonding and discussed water-mediated glassy states and double glass transition [11].

In the present study, we investigate the desorption process of the [DEME][$BF_4$]-$H_2O$ mixture. *In situ* observations reveal that the mixing state in the water-rich region became thermally unstable, and the mixing state has an important correlation with density and structural anomalies.

## 2. Experiments

We selected [DEME][$BF_4$] (Kanto Chemical Co.) as an RTIL (Figure 1). Because this RTIL is hydrophilic, 126 ppm $H_2O$ was included in the as-received sample by the Karl-Fischer titration method (870 KT Titrino plus, Metrohm AG). For $H_2O$ mixtures, we used distilled water (Wako Pure Chemical Co.). The mixtures were prepared by dissolving RTILs in a dry box under a flow of helium gas to exclude atmospheric $H_2O$. The sample solutions were simply prepared by dissolving $H_2O$ in [DEME][$BF_4$].

*In situ* observations were carried out using simultaneous X-ray diffraction and DSC measurements. The DSC was attached to a vertical goniometer with 2 kW X-ray generator (RINT-Ultima III, Rigaku Co.). For *in situ* observations of a liquid state, a sample stage was fixed horizontally with a sealed X-ray tube and a scintillation counter moving simultaneously. A parallel beam was obtained by a parabolic multilayer mirror. A long Soller slit was placed in front of the scintillation counter. Cu K$\alpha$ radiation ($\lambda = 0.1542$ nm) was selected for the simultaneous measurements. Here the scattering vector, $Q$, is defined as $4\pi(\sin\theta)/\lambda$ ($nm^{-1}$). Relative humidity (RH) was controlled by a water vapor generator (HUM-1, Rigaku Co.), which was directly connected to the DSC. Moisture inside the DSC cell was stable within ±2%RH throughout the entire desorption process.

Liquid density of the mixtures was measured with a density/specific gravity meter (DA-645, Kyoto Electronics Manufacturing Co.). The temperature range was 0–90°C. Accuracies of density and temperature were estimated to be $\pm 5 \times 10^{-5}$ g/cm$^3$ and ±0.03°C, respectively.

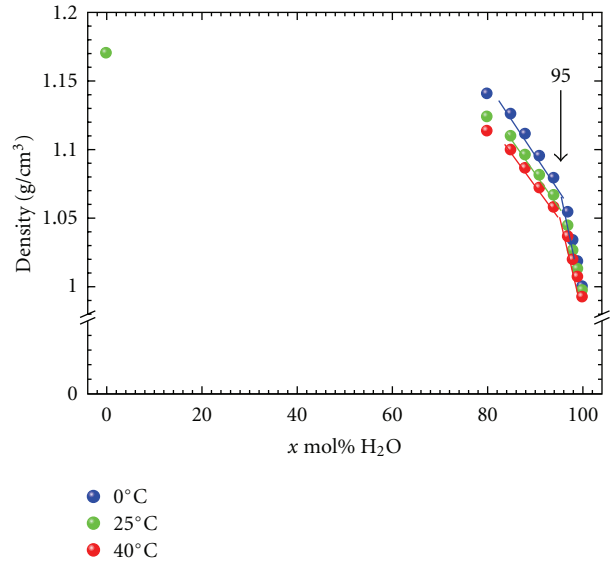


Figure 2: Temperature and concentration dependences of density in [DEME][$BF_4$]-$x$ mol% $H_2O$ mixtures.

## 3. Results

The liquid density of [DEME][$BF_4$]-$H_2O$ mixtures was measured from 40 to 0°C in the water-rich region (Figure 2). At a fixed temperature, density as a function of water concentration ($x$ mol% $H_2O$), $\rho(x)$, exhibited a sharp bend at 95 mol%. The two different gradients $(\partial\rho/\partial x)_T$ between $\rho(x < 95$ mol%) and $\rho(x > 95$ mol%) suggest that molecular packing is not described by a simple superposition of [DEME][$BF_4$] and $H_2O$ molecules. On the other hand, at fixed concentrations, a substantially different temperature dependence of density, $(\partial\rho/\partial T)_x$, was observed below and above 95 mol%. For example, $\rho(T)$ below 95 mol% depended remarkably on temperature, while the temperature dependence above 95 mol% was small. The volumetric thermal expansion coefficient, $\beta$, can enhance these density changes.

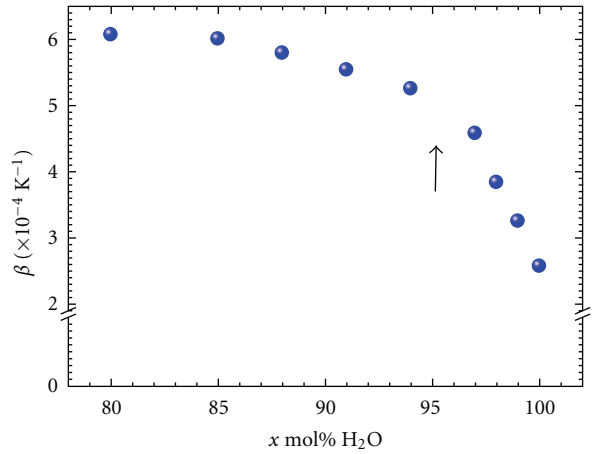


FIGURE 3: Concentration dependence of volumetric thermal expansion coefficient, $\beta$, at 25°C.

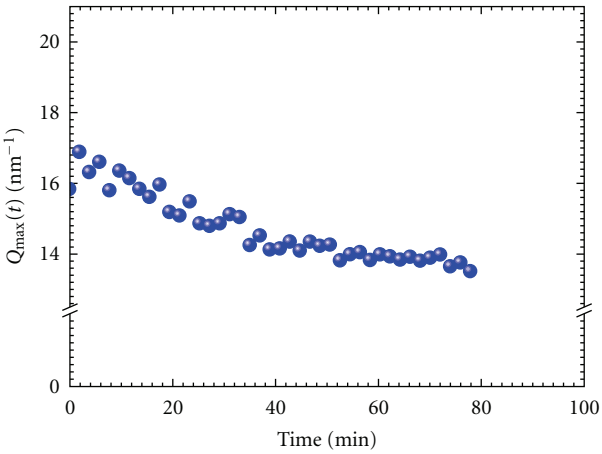


FIGURE 4: Time dependence of $Q_{max}$ position.

In general, $\beta$ is provided by $-(1/\rho)(\partial\rho/\partial T)_x$. Concentration dependence of $\beta$ at 25°C is shown in Figure 3. Note that the distinct change at 95 mol% is revealed more clearly.

Simultaneous X-ray diffraction and DSC measurements were performed at the fixed temperature (33°C) and humidity (30%RH). The initial and final water concentrations were determined to be 93.0 and 18.1 mol%, respectively, by an electric balance. In the same manner as that detailed in a previous study [12], $Q$ positions at the maximum in X-ray diffraction patterns, $Q_{max}$, were calculated by the least square fitting method using the pseudo-Voigt function. Time dependence of $Q_{max}$ at the fixed temperature is shown in Figure 4. Apart from $Q_{max}(t)$ in the present study, the $Q_{max}$-$x$ mol% plot values in [DEME][$BF_4$]-$H_2O$ mixtures were previously obtained (Figure 5) [12]. For further analysis, we represented the $Q_{max}$-$x$ relationship by a simple equation:

$$x = [1 - \exp\{-1.7(Q_{max} - Q_0)\}] \times 100. \quad (1)$$

$Q_0$ is the constant value determined to be 13.5 $nm^{-1}$ by the nonlinear fitting method. The solid curve in the

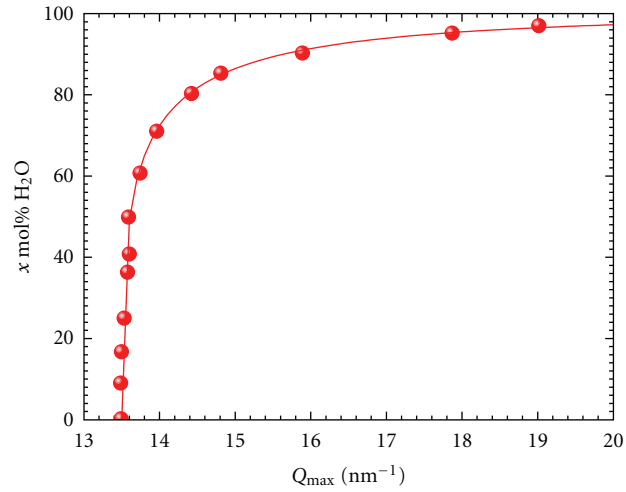


FIGURE 5: $x$-$Q_{max}$ relationship. Solid curve is obtained by the least square fitting method.

figure indicates the fitted values obtained using (1). To obtain time-dependent concentrations, the experimentally obtained $Q_{max}(t)$ values were transformed into $x(t)$ using (1) (Figure 6(a)). Here the solid curve in Figure 6(a) was obtained by the least square fitting method of a polynomial. For the quantitative analysis of the DSC thermograph, time dependence of mass during the desorption process is required. Therefore, we assumed that the mass of RTIL, $m_{IL}$, in the mixture could not decrease during the desorption process. Thus, the mass of water as a function of time, $m_w(t)$, was evaluated easily from $x(t)$ at fixed $m_{IL}$. In fact, even under vacuum (400 Pa), the mass of [DEME][$BF_4$] including various types of additives did not decrease for 48 hours [13]. Therefore, the total mass curve, $m(t)$, is given by

$$m(t) = m_{IL} + m_w(t). \quad (2)$$

Figure 6(b) shows the total mass curve, $m(t)$, which was obtained by satisfying (2). The final water concentration (18.1 mol%), which was measured by an electric balance after the desorption process, remarkably coincided with the calculated $m(t)$ within the experimental error.

In addition to the X-ray diffraction measurement for the estimation of water concentration, the DSC thermogram with time evolution was measured via *in situ* observations. As mentioned previously, the total mass decreased with increasing desorption time. Thus, we corrected the thermogram trace by $m(t)$ in Figure 6(b). As a result, we obtained a normalized heat flow as shown in Figure 7. Here $x_c$ (85 mol% $H_2O$) was the crossover concentration, which was determined by the hierarchy structure in [DEME][$BF_4$]-$H_2O$ mixtures [10]. At around $x_c$, the heat flow apparently exhibited the minimum value on the thermogram. To check an experimental error in the heat flow, the DSC trace having a little mass change, $\Delta m$, is plotted in Figure 8, where $\Delta m/m$ during desorption process was estimated to be less than 10%. Data as background were collected at 30°C and 85%RH. Both intensity and $Q$ position of the principal peak were almost constant during the measurements. Compared with the background, it is clear that the heat flow on desorption

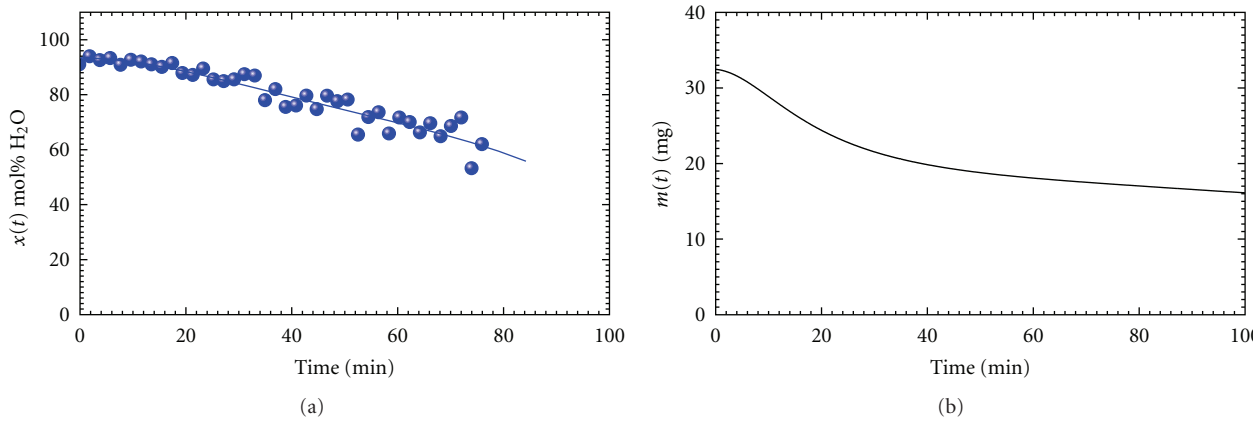


Figure 6: Time dependences of (a) water concentrations and (b) mass.

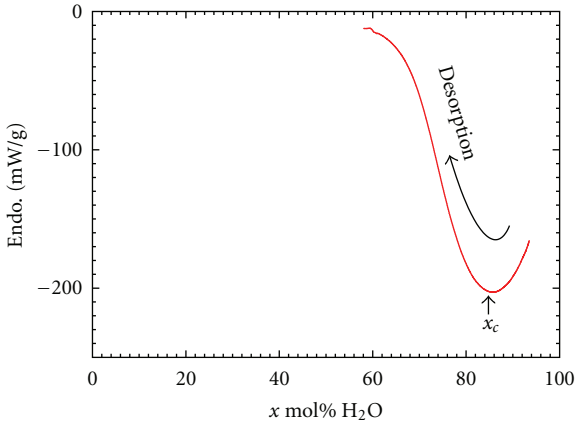


Figure 7: Water concentration dependence of normalized heat flow.

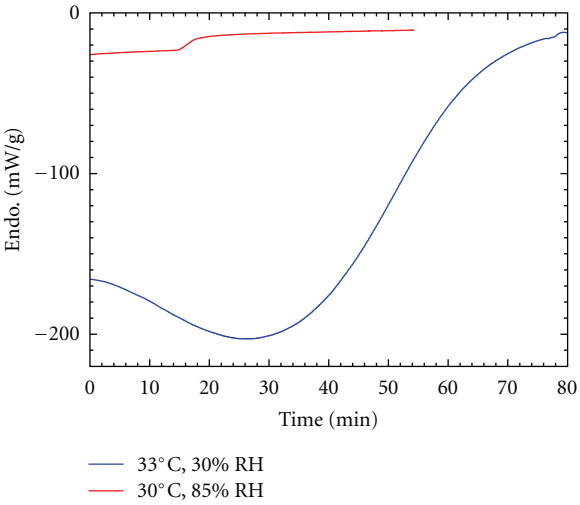


Figure 8: Time dependence of the normalized heat flow. For a comparison, the normalized heat flow at 30°C and 85%RH is plotted as background, where a little mass change was measured after the DSC scan.

process (33°C and 30%RH) has the distinct endothermic peak.

## 4. Discussion

We have shown the anomalous behavior of [DEME][$BF_4$]-$H_2O$ mixtures with respect to density and the DSC trace in Figures 2 and 7, respectively. Including the structural property obtained in a previous study [10, 12], these anomalies are summarized as follows: (i) medium-range order (MRO) develops at 85 mol% $< x <$ 95 mol% as a structural property; (ii) a crossover point from RTIL to water is observed in 85 mol% ($x_c$) by X-ray diffraction patterns; (iii) density as a function of concentration is decomposed into two regions such as $\rho(x <$ 95 mol%) and $\rho(x >$ 95 mol%); (iv) by fixing $x$ below 95 mol%, density, $\rho(T)$, highly depends on temperature; (v) at the fixed temperature, the DSC trace exhibits an endothermal peak at around $x_c$.

To explain these anomalies, we introduced the concept of specific aggregation, which consists of an inner core and an outer shell [14]. If aggregation exists at 85 mol% $< x <$ 95 mol%, structural anomalies (i) and (ii) can be well recognized. Aggregation can occur when a cation is isolated completely from an anion above 85 mol% and the MRO is developed by aggregation as an intermediate state. At the same time, anomaly (iii) supports the theory that $\rho(x <$ 95 mol%) is influenced by the existence of aggregation. The formation of an aggregation-mediated network suppresses the density changes as a function of water concentration. On the other hand, $\rho(x >$ 95 mol%) without aggregation tends to converge to the water density with increasing $x$. For example, the liquid structure in $ZnCl_2$-KCl mixtures is characterized by heterogeneous density fluctuations [15]. In molecular dynamics of several alkali halides, the low-density part is described by a void that exhibits MRO [16]. Next, we focused on $\rho(T)$ below 95 mol% (anomaly (iv)). In general, heterogeneous density fluctuations, which are composed of dense aggregations and voids, cause volume expansion. In the case of $\rho(T)$ below 95 mol%, appearance and disappearance of heterogeneity provide the highly changing density

according to temperature. At high temperatures, a pore part easily appears by thermal expansion. To compensate for the drastic change in density, the thermally activated aggregation (a dense part) could increase with increasing temperature. In contrast, the aggregation-assisted heterogeneity could disappear at low temperatures. In accordance with the population of the aggregation, we confirm that $\rho(T)$ below 95 mol% shows a high temperature dependence.

As a result, under isothermal holding, the DSC trace in the desorption process can also support the aforementioned theory. Anomaly (v) indicates that the endothermal peak at the fixed temperature is derived from the unstable mixing state. From 93 to 85 mol%, aggregation occurs as an intermediate state between water and RTIL. We determine that the anomalous thermal property of [DEME][$BF_4$]-$H_2O$ mixtures agrees with the density and structural anomalies such as the hierarchy structure.

This new methodology during the desorption process using simultaneous X-ray and DSC measurements was introduced and applied for the first time. Time dependence of concentration, $x(t)$, in the mixture is not generally evaluated by conventional DSC measurements because mass transfer, $m(t)$, should be determined during the desorption process for the quantitative thermal analysis. We have successfully estimated concentration in real time from X-ray diffraction patterns in the simultaneous measurements. From the perspective of thermodynamics, thermal property as a response to concentration is important for obtaining information of the stable/unstable mixing states at fixed temperatures.

## 5. Summary

[DEME][$BF_4$]-$H_2O$ mixtures have an anomalous mixing state in the water-rich region. Combined with the structural anomalies, we determined that specific aggregation could occur at 85 mol% $< x <$ 95 mol%. This water concentration is regarded as an intermediate state between water and RTIL. The thermally activated aggregation can explain the time and concentration dependences of density and the endothermic peak at around $x_c$. We conclude that energetically unstable aggregation contributes to the hierarchy structure in the [DEME][$BF_4$]-$H_2O$ system at around $x_c$.

## Acknowledgments

The authors appreciate Ms. M. Yasaka and Mr. A. Kishi of Rigaku Co. for experimental support and helpful discussions. Also, they thank Dr. T. Takekiyo, Professor H. Matsumoto, and Professor T. Arai of National Defense Academy for helpful discussions.

## References

[1] M. J. Earle and K. R. Seddon, "Ionic liquids. Green solvents for the future," *Pure and Applied Chemistry*, vol. 72, no. 7, pp. 1391–1398, 2000.

[2] H. Katayanagi, K. Nishikawa, H. Shimozaki, K. Miki, P. Westh, and Y. Koga, "Mixing schemes in ionic liquid—$H_2O$ systems: a thermodynamic study," *Journal of Physical Chemistry B*, vol. 108, no. 50, pp. 19451–19457, 2004.

[3] G. García-Miaja, J. Troncoso, and L. Romaní, "Excess enthalpy, density, and heat capacity for binary systems of alkylimidazolium-based ionic liquids + water," *Journal of Chemical Thermodynamics*, vol. 41, no. 2, pp. 161–166, 2009.

[4] U. Domańska, "Solubilities and thermophysical properties of ionic liquids," *Pure and Applied Chemistry*, vol. 77, no. 3, pp. 543–557, 2005.

[5] A. Riisager, R. Fehrmann, R. W. Berg, R. Van Hal, and P. Wasserscheid, "Thermomorphic phase separation in ionic liquid-organic liquid systems—conductivity and spectroscopic characterization," *Physical Chemistry Chemical Physics*, vol. 7, no. 16, pp. 3052–3058, 2005.

[6] U. Domańska and L. M. Casás, "Solubility of phosphonium ionic liquid in alcohols, benzene, and alkylbenzenes," *Journal of Physical Chemistry B*, vol. 111, no. 16, pp. 4109–4115, 2007.

[7] T. Sato, G. Masuda, and K. Takagi, "Electrochemical properties of novel ionic liquids for electric double layer capacitor applications," *Electrochimica Acta*, vol. 49, no. 21, pp. 3603–3611, 2004.

[8] Y. Imai, H. Abe, T. Goto, Y. Yoshimura, Y. Michishita, and H. Matsumoto, "Structure and thermal property of *N*, *N*-diethyl-*N*-methyl-*N*-2-methoxyethyl ammonium tetrafluoroborate-$H_2O$ mixtures," *Chemical Physics*, vol. 352, no. 1–3, pp. 224–230, 2008.

[9] H. Abe, Y. Yoshimura, Y. Imai, T. Goto, and H. Matsumoto, "Phase behavior of room temperature ionic liquid—$H_2O$ mixtures: *N*, *N*-diethyl-*N*-methyl-*N*-2-methoxyethyl ammonium tetrafluoroborate," *Journal of Molecular Liquids*, vol. 150, no. 1–3, pp. 16–21, 2009.

[10] M. Aono, Y. Imai, Y. Ogata et al., "Anomalous mixing state in room-temperature ionic liquid-water mixtures: *N*, *N*-diethyl-*N*-methyl-*N*-(2-methoxyethyl) ammonium tetrafluoroborate," *Metallurgical and Materials Transactions A*, vol. 42, no. 1, pp. 37–40, 2011.

[11] A. Kokorin, Ed., *Ionic Liquids: Theory, Properties, New Approaches*, InTech, 2011.

[12] H. Abe, Y. Imai, T. Takekiyo, and Y. Yoshimura, "Deuterated water effect in a room temperature ionic liquid: *N*, *N*-diethyl-*N*-methyl-*N*-2-methoxyethyl ammonium tetrafluoroborate," *Journal of Physical Chemistry B*, vol. 114, no. 8, pp. 2834–2839, 2010.

[13] H. Abe, T. Mori, R. Abematsu et al., submitted to *Journal of Molecular Liquids*. In press.

[14] M. Aono, Y. Imai, H. Abe, H. Matsumoto, and Y. Yoshimura, *Thermochimica Acta*. In press.

[15] D. A. Allen, R. A. Howe, N. D. Wood, and W. S. Howells, "The structure of molten zinc chloride and potassium chloride mixtures," *Journal of Physics Condensed Matter*, vol. 4, no. 6, article 005, pp. 1407–1418, 1992.

[16] M. Salanne, C. Simon, P. Turq, and P. A. Madden, "Intermediate range chemical ordering of cations in simple molten alkali halides," *Journal of Physics Condensed Matter*, vol. 20, no. 33, Article ID 332101, 2008.